

Spectroscopic and hydrodynamic characterization of DNA-linked gold nanoparticle dimers in solution using two-photon photoluminescence

Johanna Midelet,¹ Anne Débarre,² Afaf H. El-Sagheer,³ Tom Brown,³
Antonios G. Kanaras,^{1,*} Martinus H.V. Werts^{4,*}

¹ *University of Southampton, Physics and Astronomy, Faculty of Physical Sciences and Engineering, Southampton SO171BJ, United Kingdom*

² *École normale supérieure de Cachan, CNRS, lab. Aimé-Cotton and PPSM, 61 Av. du Président Wilson, F-94235 Cachan, France*

³ *University of Oxford, Department of Chemistry, 12 Mansfield Road, Oxford, OX1 3TA, United Kingdom*

⁴ *École normale supérieure de Rennes, CNRS, lab. SATIE, Av. R. Schuman, Campus de Ker Lann, F-35170 Bruz, France*

* correspondence to: a.kanaras@soton.ac.uk, martinus.werts@ens-rennes.fr

Abstract

Two-photon photoluminescence (TPPL) emission spectra of DNA-gold nanoparticle (AuNP) monoconjugates and corresponding DNA-linked AuNP dimers were obtained via photon time-of-flight spectroscopy (PTOFS). This technique is combined with two-photon photoluminescence fluctuation correlation spectroscopy (TPPL-FCS) to simultaneously monitor the optical and hydrodynamic behavior of these nano-assemblies in solution, with single particle sensitivity and microsecond temporal resolution. In this study, the AuNPs have an average core diameter of 12 nm which renders their dark-field plasmonic light scattering too weak for single-particle imaging. While the optical extinction, scattering and

photoluminescence spectra of the DNA-AuNP nanoparticles do not show sufficient difference between monomers and dimers as a result of lack of plasmonic coupling in the dimers, we find that combined TPPL-FCS enables distinction between AuNP monomers and AuNP dimers in solution by measurement of their hydrodynamic rotational and translational diffusion.

Introduction

Deoxyribonucleic acid (DNA) is a versatile building block for the nanoscale engineering of nanoparticle-based materials.^[1] Since the introduction of thiolated oligonucleotides as linkers for gold nanoparticle assembly^[2,3] various potential applications of oligonucleotide-functionalized nanoparticles in nanomedicine,^[4] metamaterials^[5] and nanoelectronics^[6] have been investigated. Plasmonic gold nanoparticles exhibit specific optical and electronic properties depending on their size, shape and arrangement.^[7] Thus, their assemblies could be described as 'plasmonic molecules'^[8,9] with adjustable response correlated to their unique structures.

Conceptually, nanoparticle dimers are the simplest example of assembled structures of nanoparticles. They have been extensively studied as sensors or plasmonic rulers using absorbance or scattering spectroscopy.^[10–12] However, a key disadvantage of these spectroscopic methods is that they cannot effectively detect the interactions between the nanoparticles when the interparticle distance is too large or when the particles are too small in size. The localised surface plasmon resonance becomes progressively damped for small particles (<30 nm) drastically decreasing the light scattering response of these particles. Such particles may be considered 'weakly plasmonic'. For instance, at the plasmon resonance peak maximum, 20 nm gold nanospheres (AuNP) scatter less than 1% of the incident photons.^[13]

For biomedical applications of such gold nanoparticles, it is particularly important to get a better understanding of their interactions with cells and complex biological structures, which requires the ability to track their location and distribution in these systems.^[14] Often, the method used to image and track gold nanoparticles in cells is dark field microscopy, which has recently been extended to hyperspectral^[15] and SERS^[16] imaging. Although these imaging methods are essential they are hampered by the lower limit on the size of metal nanoparticles they can detect.

Here we demonstrate an alternative method for tracking DNA oligonucleotide-coated nanoparticles in liquid media by combining multiphoton-excited emission spectroscopy and fluctuation correlation spectroscopy (FCS). Whereas multiphoton-excited photoluminescence fluctuation correlation spectroscopy of individual luminescent silicon nanoparticles^[17] and individual gold nanoparticles^[18] have been reported, the applicability of FCS to assemblies of nanoparticles has not yet been explored.

In the present work, two-photon photoluminescence (TPPL) emission spectra of DNA-gold nanosphere assemblies are obtained via photon time-of-flight spectroscopy^[19,20] (PTOFS). It is shown that two-photon-excited emission spectroscopy detects plasmonically small (12 nm averagediameter) gold nanospheres with single-particle sensitivity, and probes their localized surface plasmon resonance spectrum, circumventing the problem of the very weak dark-field light scattering signal of these particles. The TPPL spectroscopy is then extended to two-

photon photoluminescence fluctuation correlation spectroscopy (TPPL-FCS), yielding a sensitive measurement that simultaneously probes the plasmonic spectroscopy and the hydrodynamics of nano-assemblies. Our work opens interesting opportunities for detection, imaging and *in situ* characterization of molecularly linked nanoparticle assemblies, and may offer a new optical read-out mode for nanoparticle-based nucleic acid detection.

The experiments were carried out on a collection of well-defined 12 nm AuNP-DNA monoconjugates and corresponding linked AuNP dimers. Monofunctionalization of gold nanospheres with four different single-stranded DNA (ssDNA) strands generates four "monomers": AuNP-A, AuNP-B, AuNP-C, AuNP-D. Two DNA-linked dimers are then obtained by hybridisation of the complementary DNA sequences,: the 'short-link' dimer AD (26 base-pair (bp) interparticle distance) and the 'long-link' dimer BC (146 bp). The collection of 4 AuNP-monoconjugates and 2 dimers is schematized in Figure 1.

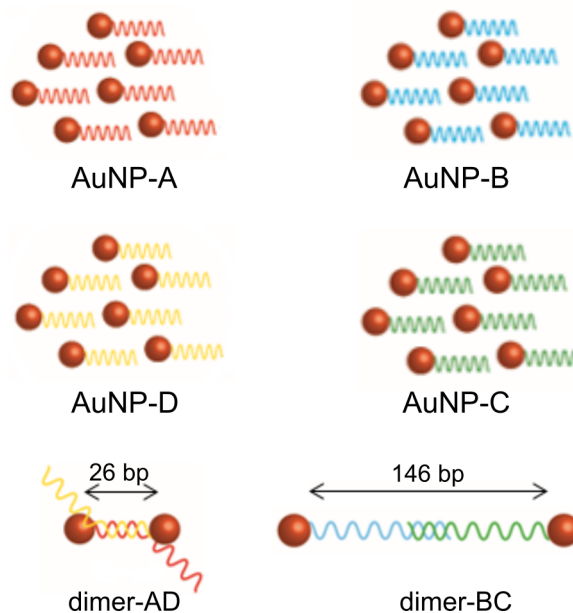


Figure 1. Single-stranded DNA-gold nanosphere monoconjugates (AuNP-A, AuNP-B, AuNP-C, AuNP-D), and the corresponding DNA-linked dimers with interparticle links of 26 ('short link' AD) resp. 146 bp ('long link' BC).

Results and discussion

Optical extinction and scattering spectra

The linear optical extinction spectra of the ssDNA-AuNP monoconjugates and the DNA-linked AuNP dimers are all very similar in shape, displaying the well-known plasmonic resonance near 520 nm for 12 nm AuNP (Figure 3). The short-link dimer AD and long-link dimer BC do not show any significant alteration of the plasmon resonance band compared to

the monomers. This is illustrated by the position of the extinction maximum, which is found to be consistently at 521 nm (Table 1).

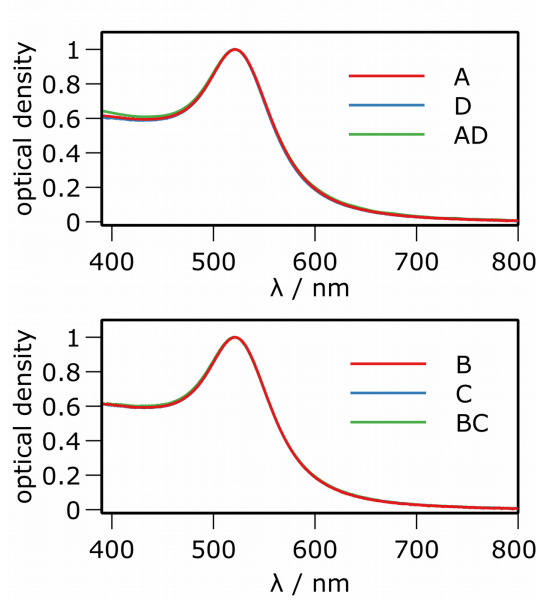


Figure 3. Normalized extinction spectra of ssDNA-gold nanoparticle monoconjugates and their resulting DNA-linked dimers in aqueous solution, average gold core diameter 12 nm. Top: short-link dimer AD; Bottom: long-link dimer BC. There is virtually no difference in the extinction spectra of the monomer AuNP and the dimers.

From the similarity of the extinction spectra between monomers and dimers, we infer that there are no significant plasmonic interactions between the constituent gold nanospheres in the dimer. The absence of significant plasmonic interaction indicates that the interparticle distance in both types of dimers AD and BC is too large for such interaction to occur. It has been demonstrated that such plasmonic interaction critically depends on the interparticle gap and also on the nanoparticle diameters.^[21–24] Jain et al.^[21] found that the fractional wavelength shift $\Delta\lambda/\lambda_0$ of the plasmon band in homodimers depends on the particle diameter d and the surface-to-surface gap s

$$\frac{\Delta\lambda}{\lambda_0} \approx 0.18 \exp\left(\frac{-(s/d)}{0.23}\right) \quad (1)$$

Based on this formula, we estimate that for the 12 nm diameter gold nanospheres used here, interparticle gaps beyond half that length (6 nm) lead to undetectable plasmonic interaction.

Table 1. Spectroscopic data. Linear optical extinction and scattering maxima ($\lambda_{\max}^{\text{ext}}$ resp. $\lambda_{\max}^{\text{sca}}$), and scattering yield at the wavelength of maximum scattering cross section ($\phi_{\text{sca}}^{\text{max}}$). Wavelength of maximum two-photon photoluminescence (TPPL) emission ($\lambda_{\max}^{\text{TPPL}}$)

	extinction	scattering		TPPL (λ_{exc} 800 nm)
	$\lambda_{\max}^{\text{ext}}$ [nm]	$\lambda_{\max}^{\text{sca}}$ [nm]	$\phi_{\text{sca}}^{\text{max}}$	$\lambda_{\max}^{\text{TPPL}}$ [nm]
AuNP-A	521	542	3×10^{-3}	538
AuNP-D	521	542	3×10^{-3}	539
'short-link' dimer AD	521	546	4×10^{-3}	547
AuNP-B	521	546	4×10^{-3}	539
AuNP-C	521	541	3×10^{-3}	533
'long-link' dimer BC	521	545	5×10^{-3}	550

In addition to light extinction, nanoparticles (NP) and NP assemblies display light scattering, depending on their shape, size, and core material. Light scattering provides further information on the plasmonic properties of the objects. As described previously,^[13,23] a corrected light scattering spectrum of a nanoparticle solution can be obtained in a conventional right-angle fluorimeter configuration using white light as the illumination source, and correcting the raw sample light scattering spectrum $I_{\text{raw}}(\lambda)$ using the spectrum of a Ludox reference sample $I_{\text{raw}}^{\text{Ludox}}(\lambda)$ according to Equation (2)

$$I_{\text{LS}}(\lambda) = \lambda^{-4} \frac{I_{\text{raw}}(\lambda)}{I_{\text{raw}}^{\text{Ludox}}(\lambda)} \quad (2)$$

Sufficiently diluted Ludox is a good light scattering reference since it is a perfect Rayleigh scatterer.^[25] In order to account for batch-to-batch variations in the Ludox concentration, the Ludox reference sample is characterised by an optical density parameter p_0 such that each of their extinction spectra is described by Equation (3).

$$\text{OD}_{\text{Ludox}}(\lambda) = p_0 \lambda^{-4} \quad (3)$$

While the corrected light scattering spectrum $I_{\text{LS}}(\lambda)$ has the spectral shape of the scattering cross section spectrum and does not depend on any instrumental parameters, its intensity still does depend on the nanoparticle concentration, which is usually not precisely known for purified nanoparticle solutions. Here, we propose to normalize the corrected light scattering spectrum using the Ludox density parameter p_0 and the optical density OD of the nanoparticle sample at the wavelength $\lambda_{\max}^{\text{LS}}$ where its scattering I_{LS} is maximal (Equation 4).

$$I_{\text{QENLS}}(\lambda) = \frac{p_0 I_{\text{LS}}(\lambda)}{\text{OD}(\lambda_{\max}^{\text{LS}})} \quad (4)$$

It can be readily shown that $I_{\text{QENLS}}(\lambda)$ reproduces the shape of the light scattering cross section spectrum $\sigma_{\text{sca}}(\lambda)$, and that its maximum gives the scattering (quantum) efficiency $\sigma_{\text{sca}}/\sigma_{\text{ext}}$ at that wavelength.

$$I_{\text{QENLS}}(\lambda) = \frac{\sigma_{\text{sca}}(\lambda)}{\sigma_{\text{ext}}(\lambda_{\text{max}}^{\text{LS}})} \quad (5)$$

We call this the quantum-efficiency normalized light scattering (QENLS) spectrum. It describes the intrinsic light scattering behavior of the nanoparticle in solution, independent of concentration, specific illumination or spectrometer properties. It allows light scattering of different nanoparticles to be compared directly, both in terms of the spectral shape and the scattering efficiency.

As stated above, the concentration independence is interesting for nanoparticle characterization, since it is often difficult to precisely know the concentration of nanoparticle sample preparations. Moreover, QENLS spectra may be obtained theoretically from the scattering and extinction cross section spectra, calculated using analytic^[26] or numerical^[27–32] electromagnetic models. This allows for a direct comparison between experiment and theoretical model and help in establishing structure-property relations for these plasmonic assemblies.

Figure 4 shows the QENLS spectra of the purified ssDNA-AuNP monoconjugates and DNA-linked dimers in pure water. The scattering efficiency is low, below 1%, as expected for 'plasmonically small' gold nanoparticles. While the scattering by the nanoparticles is weak, it can still be discerned in the light scattering spectrum by the plasmon-resonant band near 540 nm. We emphasize that these spectra are obtained from diluted bulk solutions in cuvettes using a bright white light source and are not single-particle spectra. The measurement of this weak scattering is relatively sensitive to even minor quantities of scattering impurities and tiny air bubbles. Care was taken to avoid these, by careful filtration and also by letting the samples rest and equilibrate before measurement.

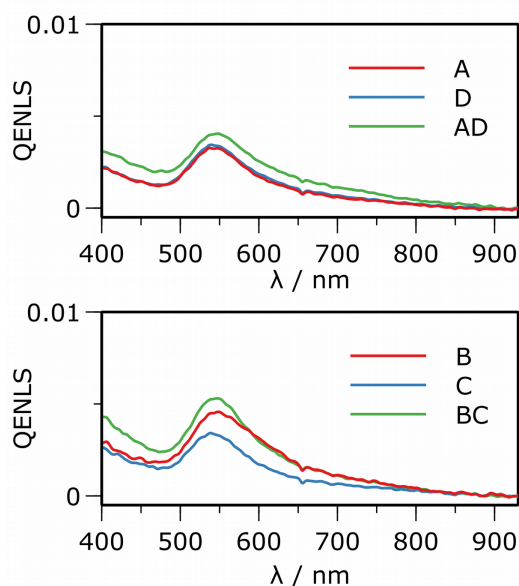


Figure 4. Quantum-efficiency normalized light scattering (QENLS) spectra of ssDNA-AuNP monoconjugates and their corresponding DNA-linked dimers in aqueous solution. Top: AD dimer; Bottom: BC dimer.

The experimental scattering efficiencies at the scattering maximum are included in Table 1, and are between 3×10^{-3} and 5×10^{-3} . A simple, idealized calculation on isolated 12 nm diameter perfect gold nanospheres in a medium of refractive index 1.33 (water) using Mie theory (see Supporting Information) yields 2×10^{-3} , which is close to the experimental values. The experimental values are marginally higher than the theoretical values, due to the particle size distribution, deviations from spherical shape, and local refractive index effects due to the ligand shell, which were not taken into account in the simple theoretical model. The Mie calculation furthermore confirms the spectral shape of the QENLS spectrum (Supporting Information, Figure S5). This demonstrates the relevance of the QENLS spectrum for the characterisation of plasmonic nanostructures in solution.

There is very little difference in the light scattering by the DNA-linked AuNP dimers compared to the 'monomer' ssDNA-AuNPs monoconjugates. Like the extinction spectra, the scattering spectra do not show any features indicating strong plasmonic interaction between the nanoparticles in these dimer structures. The DNA linkers create interparticle distances that are too large for such plasmonic interactions to occur. As discussed above, plasmonic interactions critically depend on interparticle distance and the plasmonic properties of the particles.

Microfluidic measurement of diffusion coefficients

In order to ensure that the absence of changes in the extinction and scattering spectra was not due to unexpected dissociation of the dimers, we studied the diffusion behavior of the nanoparticle dimers in solution. We modified our previously described^[33] microfluidic method for measuring diffusion coefficients to include a spectroscopic flow cell. The method is based on measuring the diffusive mass transfer from the nanoparticle solution to the pure solvent, which are in parallel laminar flow at a specified flow rate in the central channel of microfluidic 'H'-circuitry. The experiment and analysis were made more convenient with respect to our prior work by directly determining diffusion coefficients from individual optical extinction measurements at selected flow rates. The protocol is described in the experimental section.

The diffusion coefficients obtained through microfluidic measurement are collected in the first column of Table 2. Compared to small molecules, the diffusion of the gold nanoparticles is at least an order of magnitude slower, and this requires very low flow rates in our set-up. We found that these were difficult to stabilize, and prolonged times were necessary to reach a stationary state after changing the flow rate. This explains the large error bars, which handicaps in particular the determination for dimer-BC. The stability of the microfluidic measurement can be improved by further temperature stabilization, use of pressure-driven flow instead of syringe pumps, and reduction of dead volume by integrating the observation flow cell in the microfluidic structure.

In spite of this experimental difficulty, we observe that the diffusion coefficient of bis-sulfonato(phenyl)-phenylphosphine (BSPP)-coated AuNPs is in line with the value expected for a 13 nm diameter sphere (12 nm core + 0.5 nm ligand shell), using the Stokes-Einstein-Sutherland relation, *i.e.* $3.8 \times 10^{-11} \text{ m}^2 \text{ s}^{-1}$. Moreover, we observed that ssDNA-AuNP monoconjugates have a significantly lower diffusion coefficient than BSPP-AuNP. The diffusion coefficient is further reduced in the case of a dimer.

Table 2. Translational diffusion coefficients from microfluidics and from TPPL-FCS. Temperature was 298 K.

	microfluidics $D_{\text{trans}} (\text{m}^2 \text{ s}^{-1})$	TPPL-FCS $D_{\text{trans}} (\text{m}^2 \text{ s}^{-1})$
AuNP-BSPP	$4.1 (\pm 1.3) \times 10^{-11}$	n.m.
AuNP-A	$2.0 (\pm 0.8) \times 10^{-11}$	$2.3 (\pm 0.2) \times 10^{-11}$
AuNP-B	n.m.	$2.0 (\pm 0.1) \times 10^{-11}$
AuNP-C	n.m.	$2.3 (\pm 0.2) \times 10^{-11}$
AuNP-D	n.m.	$2.2 (\pm 0.2) \times 10^{-11}$
short-link dimer AD	n.m.	$1.6 (\pm 0.1) \times 10^{-11}$
long-link dimer BC	$0.6 (\pm 0.5) \times 10^{-11}$	$1.1 (\pm 0.3) \times 10^{-11}$

n.m. = not measured

Two-photon photoluminescence

The DNA-linked AuNP dimers cannot readily be distinguished from the ssDNA-AuNP monoconjugates when steady-state light extinction and scattering spectroscopies are used. Straightforward detection of the dimers is further complicated by their weak light scattering. Microfluidic measurement of diffusion coefficients does indeed distinguish (hydrodynamically) between monomer and dimer, but this requires a separate experiment. In the following we will show that the intrinsic multiphoton-excited luminescence from the AuNP monomers and dimers in solution provides a more sensitive and rapid "one pot" method for detecting and characterising such samples.

Upon excitation of the nanoparticle solutions with 200 fs pulses of 800 nm light from a Ti-sapphire laser (76 MHz repetition rate, 4.5 mW average power on the sample, 60x NA 1.2 water immersion objective), an upconverted emission band is observed in the 450-700 nm range. This emission is attributed to two-photon excited photoluminescence (TPPL).^[18,34,35] The TPPL of all monomers and dimers studied is very similar, in terms of spectral shape and in terms of intensity, which is always in the same order of magnitude, varying within a factor of 2. Small differences in TPPL emission intensity between samples were observed, but these were not characterized and studied in detail.

In **Figure 5** we show the TPPL spectra for the DNA-linked AuNP dimers, obtained using photon time-of-flight spectroscopy^[18,19] (PTOFS). The TPPL emission is a broad band peaking near 540 nm, and reproduces the spectral shape of the linear light scattering spectrum. Such spectral similarity between photoemission and resonant light scattering is a general observation with plasmonic nanostructures.^[19,36,37]

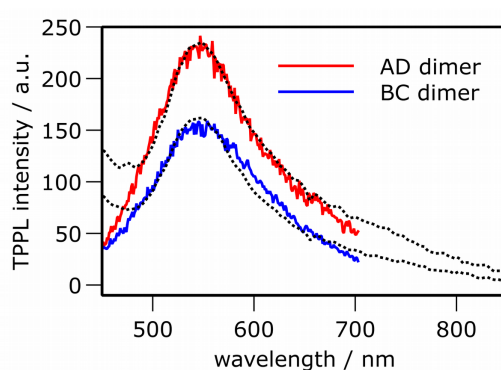


Figure 5. Two-photon photoluminescence spectra from DNA-linked dimers (concentration 3.5 nM in water, excitation: 800 nm, 76 MHz, 200 fs pulses). The dotted lines are the corresponding linear light scattering spectra, scaled for comparison.

The mechanisms underlying light emission by plasmonic nanostructures are still under debate, both for Stokes ('one-photon excitation')^[19,36,38,39] and anti-Stokes upconversion ('multi-photon excitation')^[14,18,40] emission that have been observed for plasmonic nanostructures. The TPPL mechanism has been far less studied in comparison to one-photon excited photoluminescence (OPPL). Similarly to OPPL, the resemblance of the luminescence spectra with the corresponding scattering spectra suggests that the mechanism is plasmon-mediated. In a first step, a two-photon absorption process excites an electron from the *d*-band to the *sp*-band. Two models have been suggested for the mechanism of photon emission. In the first model, the emission results from the interband electron-hole recombination, which is amplified at the frequencies of the surface plasmon.^[41,42] In the second one, luminescence originates from the radiative intraband deexcitation of the surface plasmons.^[43,44]

However, recent work^[45] suggested that the term 'photoluminescence' should not apply, as the light emission - in the case of plasmonic structure displaying very small interparticle gaps - might originate from an inelastic scattering process. Such a process would be similar to Raman scattering, with the difference that hot electrons in the gradient plasmon field mediate the energy exchange, instead of the vibrations that fulfill this role in 'standard' Raman scattering. The theoretical model from that work predicts a 100-fold increase in (one-photon excited) light emission going from monomer to dimer, which is not in agreement with experimental observations where monomers and dimers display similar light emission intensities.^[38,39] Interestingly, the authors do suggest interband-mediated photoluminescence (PL) to be operative in monomeric plasmonic particles.

Agnostic about the exact photophysical mechanism, we choose to refer to the upconverted light emission observed under multi-photon excitation conditions as "two-photon excited photoluminescence" (TPPL), which is also the term most regularly used in recent literature to refer to this phenomenon. Also, for most practical reasons, the laser-excited light emission is indistinguishable from two-photon excited fluorescence. However, we do acknowledge that "upconverted light emission" may be a more fitting and general term.

A particularly attractive feature of the confocal measurement of TPPL in our set-up is the possibility to simultaneously obtain information on the hydrodynamics of the particles by analyzing the TPPL intensity fluctuations in the confocal volume due to Brownian motion, *i.e.* performing TPPL fluctuation correlation spectroscopy (TPPL-FCS). TPPL-FCS is like fluorescence correlation spectroscopy,^[46–48] but instead of (monophotonic) fluorescence it uses the multi-photon excited light emission from the plasmonic structures for probing the dynamics of the confocal volume. Excitation of the intrinsic luminescence of the plasmonic structure is a useful alternative to the introduction of molecular fluorescent tags^[49–51] in the structures. One-photon excited photoluminescence FCS has recently been applied to study the hydrodynamics of gold nanorods via their intrinsic photoexcited light emission.^[37]

Typical TPPL-FCS results for a ssDNA-AuNP monoconjugate and the corresponding DNA-linked AuNP dimer are shown in Figure 6. The autocorrelation curves of the TPPL intensity in the confocal observation volume clearly display different shapes between the AuNP-B monoconjugate and the AuNP dimer.

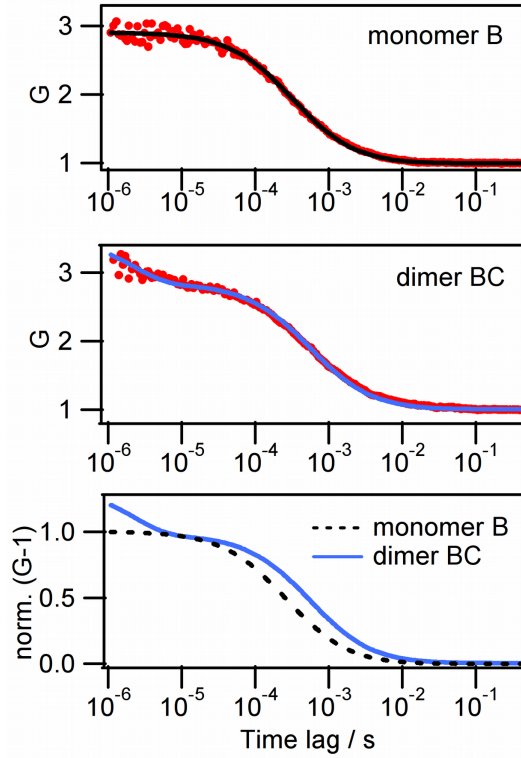


Figure 6. TPPL-FCS (excitation 800 nm, 4.5 mW). Top and middle: TPPL intensity autocorrelation correlation curves for ssDNA(B)-AuNP monoconjugate and long-link dimers BC, and fit using translational and rotation-translational diffusion respectively. Bottom: best fits for monomer and dimer TPPL autocorrelation, rescaled to enable direct comparison, demonstration the longer translational time of the dimers and the presence of a rotational component at short time lag.

The autocorrelation data for ssDNA-AuNP monoconjugates can be described using a model involving only translational diffusion (Eqn. 6), assuming a 3D Gaussian beam.

$$G(\tau) = 1 + \frac{1}{N} \left[\left(1 + \frac{\tau}{\tau_D} \right) \sqrt{1 + q \frac{\tau}{\tau_D}} \right]^{-1} \quad (6)$$

The translational diffusion time constant τ_D is directly related to the diffusion coefficient D and the lateral waist of the observation volume ω_{xy}^2 , i.e. $\tau_D = \omega_{xy}^2 / 8D$ in the case of two-

photon excitation (see Table 2). Furthermore, $q = \omega_{xy}^2/\omega_z^2$ with ω_z being the longitudinal waist of the observation volume. N is the mean number of particles diffusing simultaneously inside the excitation volume. Calibration of the focal volume using Rhodamine 6G in water gives $\omega_{xy} = 225$ nm and $q = 0.075$.

We found that the autocorrelation data for both dimers AD and BC requires a model including a rotational term, described by rotational time constant τ_R (Eqn. 7), which can also be expressed by the rotational diffusion coefficient $D_R = 1/6\tau_R$.^[52]

$$G(\tau) = 1 + [G_D(\tau) - 1] [1 + p \exp(-\tau/\tau_R)] \quad (7)$$

The rotational diffusion coefficients were found to be $D_R = 7 (\pm 0.8) \times 10^4 \text{ s}^{-1}$ for dimer-AD, and $D_R = 5.5 (\pm 0.8) \times 10^4 \text{ s}^{-1}$ for dimer-BC. There is much noise on the autocorrelation at very short time lags. This results in a sizeable uncertainty on the time constant for rotational diffusion. However, in combination with the observation of a longer diffusion time, the appearance of this rapid rotational contribution demonstrates the hydrodynamic difference between ssDNA-AuNP monoconjugates and DNA-linked dimers, due to their different sizes.

The values for the rotational diffusion coefficients D_R and the translational diffusion coefficients D_T obtained from TPEL-FCS may be compared to theoretical model values calculated for nanorods with diameter $d = 12$ nm and length $L = 33$ nm (AD) or $L = 74$ nm (BC), respectively. Following the hydrodynamic model by Tirado et al.^[53] the expressions of the translation diffusion coefficient and of the rotation constant D_R are:

$$D_T = \frac{k_b T}{3\pi\eta L} \left[\ln \left(\frac{L}{d} \right) + 0.312 + 0.565 \frac{d}{L} - 0.100 \frac{d^2}{L^2} \right] \quad (8)$$

$$D_R = \frac{3k_b T}{\pi\eta L^3} \left[\ln \left(\frac{L}{d} \right) - 0.662 + 0.917 \frac{d}{L} - 0.050 \frac{d^2}{L^2} \right] \quad (9)$$

The calculation yields $D_T = 2 \times 10^{-11} \text{ m}^2 \text{ s}^{-1}$ and $D_R = 7 \times 10^4 \text{ s}^{-1}$ for "AD-like" nanorods, and $D_T = 1.3 \times 10^{-11} \text{ m}^2 \text{ s}^{-1}$ and $D_R = 1.4 \times 10^4 \text{ s}^{-1}$ for "BC-like" nanorods. These values are in the same order of magnitude and display the same trends as those experimentally obtained for the dimers (Table 2) despite the rough approximation related to the shape of the object. The agreement with the simple model is better for AD dimer than for BC dimer. The former has the shortest linker between the two nanospheres, which may explain the better agreement. This result indicates that the hybridised DNA linker is indeed rigidly extended between the components of the structure.

The combined theoretical and experimental results on the translational diffusion coefficient of ssDNA-AuNP monoconjugates and DNA-linked AuNP dimers illustrate that the diffusion coefficient of elongated objects ($L = 33$ nm and $L = 74$ nm for a width of 12 nm) cannot be estimated simply from the Stokes-Einstein equation using the long axis as the hydrodynamic radius, but requires more elaborate hydrodynamic models. In the same vein, it has recently

been shown that attaching a single long rigid rod-shaped DNA molecule (68 bp, 23 nm) to a 6 nm diameter nanosphere leads to only a small increase in effective hydrodynamic Stokes radius (3.2 nm to 5.8 nm), well below the additional length provided by the rod-like molecule.^[54]

It is interesting to compare the translation diffusion coefficients obtained through TPPL-FCS and microfluidics (Table 2). The two methods agree fairly well. The trend in diffusion coefficient between ssDNA-AuNP monogconjugates and DNA-linked AuNP dimers, and the order of magnitude of the coefficient, are reproduced by the microfluidic measurement. It should be noted that there is a large uncertainty on the microfluidic data, in particular for dimer-BC, which was measured at very low flow rates.

Beyond this direct comparison of the determination of hydrodynamic radii by the three different measurements described here, we can also look at studies of gravitational sedimentation^[55–57] and analytical centrifigation^[54,58–60] of nanoparticle solutions. These also yield insight in the hydrodynamic behaviour of nanoparticles. Recently we studied the gravitational sedimentation of a DNA-linked dimer of 13 nm AuNPs.^[55] That dimer has a structure similar to dimer BC (but using a slightly different DNA linkage). At 277 K, we obtained $D = 0.58 \times 10^{-11} \text{ m}^2 \text{ s}^{-1}$, which — taking into account the change in viscosity of the water — would correspond to $D = 1.1 \times 10^{-11} \text{ m}^2 \text{ s}^{-1}$ at 298K, in good agreement with the values obtained by TPPL-FCS and microfluidics. In addition to the diffusion coefficient, such measurements yield the sedimentation coefficient, which also critically depends on particle shape.^[54]

Conclusion

TPPL combined with PTOFS and FCS provides a sensitive method to detect and characterize even the 'weakly plasmonic' assemblies studied here that do not efficiently scatter light, and whose plasmonic resonance does not show a clear difference between monomeric species and dimeric assemblies. In contrast to linear optical spectroscopy, which is carried out in typical spectroscopic cell volumes (3 mL), TPPL is measured in a small confocal volume, typically in the sub-picolitre range, the entire sample being a droplet ($\sim 50 \text{ }\mu\text{l}$). Such a confocal configuration is compatible with detection in capillaries, such as those found in microfluidics or analytical chromatography.

For the type of DNA-linked gold nanosphere dimers that were studied here, it is the hydrodynamic behavior measured using TPPL-FCS that carries the information allowing to distinguish between monomeric and dimeric objects. When considering potential nucleic acid detection schemes, this suggests that in particular the rotational component of the TPPL correlation function may probe the dimerization of gold nanosphere-based DNA probes upon hybridization, and transduce the presence and concentration of specific nucleic acid analytes.

Furthermore, our study shows that TPPL of small AuNPs is bright enough not only to detect and image AuNPs but also to study their spectral and hydrodynamic properties.

Experimental details

Synthesis and purification of ssDNA-AuNP monoconjugates and DNA-linked dimers

A schematic illustration of the route to make DNA-gold nanoparticle monomers and dimers is shown in [Figure S1 \(Supporting Info\)](#). In summary, four solutions of DNA-gold nanoparticle monoconjugates were prepared by mixing bis-sulfonato(phenyl)-phenylphosphine (BSPP)-coated AuNPs with one of the four thiolated ssDNA at a ratio 1:1, and subsequent purification by gel electrophoresis. The different ssDNA oligonucleotides are labeled A, B, C, D. The DNA sequences are shown in [Supporting Info, Figure S3a](#)). The DNA-gold nanoparticle monoconjugates were then mixed to create nanoparticle dimers through DNA hybridisation of the complimentary oligonucleotide strands (A + D resp. B + C).^[61] Agarose gel electrophoresis was used to purify the samples. This resulted in solutions of AuNP-dimer with a short (26 bp) DNA link (dimer-AD) and AuNP-dimer with a long (146 bp) DNA link (dimer-BC). The synthetic details and the characterization of the purified nanoparticles are given in the [Supporting Info](#).

Optical spectroscopy

Optical spectroscopy was carried out at ambient temperature (298 K) on air-equilibrated samples contained in standard 1 cm quartz or plastic fluorescence cuvettes. UV-visible extinction spectra were measured using an optical fiber-based system (Ocean Optics) incorporating a CCD spectrometer (USB4000-VIS-NIR) and a tungsten-halogen light source (LS1, 6.5 W, 3100 K) equipped with a BG34 colour correction filter.

Light scattering measurements were performed according to the methodology that we described previously.^[13,19,23] The method uses a right-angle configuration, measuring only light scattered around 90°, assuming that the angular distribution of light scattering by the samples and the reference is identical. This is valid for gold particles smaller than about 100 nm.^[62] The sample solutions were illuminated with white light (LS-1 tungsten-halogen light source). The scattered light was collected at a fixed angle of 90°, and analysed using a back-thinned CCD spectrograph (Ocean Optics QE65000). All samples were diluted such that the optical density remains well below 0.05. A solvent background was subtracted from all recorded spectra, and the background-subtracted raw spectra were corrected using Ludox as the perfect Rayleigh scatterer.^[25] In the present work, the light scattering spectra were normalized such that the maximum has the value of the scattering quantum yield at that wavelength, as explained above.

The Ludox reference sample consisted of the supernatant of a Ludox SM30 (Aldrich) suspension centrifuged for 1 h at 9700 x *g*, which was diluted 200 times in 0.05 M NaCl. For each measurement series, three Ludox reference samples were prepared, and each reference sample was characterised using its p_0 value, by fitting the function $OD_{\text{Ludox}}(\lambda) = p_0\lambda^{-4} + p_1$ to the experimental Ludox extinction spectrum. The baseline value p_1 enables for correction for very small differences in baseline, but should be very close to zero, else a new reference sample is prepared. Finally, it was verified that all three Ludox samples gave identical scattering spectra, in both shape and intensity. The average p_0 value of the three Ludox samples was used.

Where appropriate, the extinction and scattering spectra were smoothed using the Whittaker-Eilers (WE) algorithm^[63] to reduce noise and bring out more clearly the spectral shape. The WE smoother, which conserves both spectral shape and peak intensity and is simpler and more efficient than the Savitsky-Golay^[64] filter, was programmed in Python using the scientific 'numpy' and 'scipy' libraries^[65] (see [Supporting Information](#)).

Microfluidic measurement of diffusion coefficients

The microfluidic measurement of diffusion coefficient is based on the microfluidic 'H-filter'.^[66] We adapted our previously described microfluidic method for measuring diffusion coefficients^[33] to include a spectroscopic flow cell (SMA-Z-10 Ultem, FIALab Instruments, Seattle WA, USA) which was used to measure the optical extinction spectrum using the fiber-coupled spectrometer cited above. The long (1 cm) path length of the flow cells enables precise measurement of optical density (OD), even at low concentration.

The measurement is based on determining the extent of the diffusive mass transfer from the flow of nanoparticle solution to the flow of pure solvent, which are continuously injected at separate inputs of the microfluidic circuit ([Supporting Info, Figure S6](#)) and flow parallel after meeting at a 'T'-junction, enabling diffusive mass transfer to occur. At the end of the interaction zone, the flow is split in two by another 'T'-junction (thus constituting an 'H'-filter circuit). The extent of diffusive transfer between the two flows can be determined from the gain in OD of the exiting solvent flow (which will carry the subscript "B"), and/or from the loss in OD from the exiting nanoparticle solution flow (subscript "A"). We measured the OD of the solvent flow, OD_B . The extent of diffusion ξ is defined here in terms of the concentrations of nanoparticles in the flows exiting the H-filter, c_A and c_B (their sum is equal to the injected nanoparticle concentration). For a measurement of the concentration at exit "B", we have [Eqn. 10](#).

$$\xi = \frac{2c_B}{c_A + c_B} = \frac{2OD_B}{OD_{\text{tot}}} \quad (10)$$

Note that this definition is (slightly) different from the definition ξ in our initial work;^[33] the present definition leads to $\xi = 0$ in case of no diffusive transfer occurring, and to $\xi = 1$ for

diffusive transfer being complete. The overall concentration of the injected nanoparticle solution (OD_{tot}) was measured by stopping the injection of the pure solvent, causing only the pure nanoparticle solution to exit at both exits and traverse the flow cell. On the other hand, when injecting only pure solvent, the baseline for the extinction measurement was recorded.

At a given volumetric flow rate $U(\text{m}^3 \text{s}^{-1})$; this is the sum of the two entering flow rates), we can theoretically calculate the extent of diffusion ξ for a given diffusion coefficient D . For this, it is convenient to convert the flow rate into a (device-independent) measure of the interaction time, τ (Eqn. 11), using channel length L , channel width w , and channel height h .

$$\tau = \frac{\pi^2 L h}{w U} \quad (11)$$

Using the analytic solution of the diffusion equation,^[33] we obtain Eqn. 12 for the presently defined ξ . This sum has to be evaluated numerically. For sufficiently large values of $D\tau$ the series converges rapidly, in which case only a few terms are needed for a reliable result (sometimes even only the first term).^[33]

$$\xi = 1 - \sum_{i=0}^{\infty} \frac{8}{\pi^2 (2i+1)^2} \exp(-D(2i+1)^2 \tau) \quad (12)$$

When ξ has experimentally been measured at a certain specified flow rate U , D can be found by solving $\xi_{\text{exp}} - \xi_{\text{theo}}(D) = 0$ for D . This needs to be done numerically, for example using the secant method, since there is no direct inverse expression for Eqn. 12. (When only the first term of the series in Eqn. 12 is significant, there is a direct analytic inverse expression, but this feature is not used here.)

The experimental flow rates were chosen such that the measured ξ was in the range 0.1 ... 0.7. For each sample several determinations of D were carried out, at various flow rates over several days, giving access to the statistical uncertainty on the diffusion coefficient. The connection of the flow cell to the microfluidic system introduced a sizeable dead volume, which resulted in long times for the reading of the OD to stabilize, in particular at low flow rates. Drift and fluctuations during this time contribute to the relatively large confidence interval. Temperature was close to 298K, but fluctuated somewhat (± 2 K) during measurement.

The microsystem used had an interaction channel of height 140 μm , width 200 μm and length 50 mm. The precise microfluidic circuit is shown in the Supporting Info. Prior to each experiment the system was washed with Milli-Q water (200 μL) at a flow rate of 4 $\mu\text{L}/\text{min}$. Milli-Q water (Entry B) and the sample studied (Entry A) were introduced in the microsystem using two syringes ($d = 2.5$ mm) mounted on individual syringe pumps. The system was left to stabilize for one hour at the flow rate selected for each experiment (typically between 1 x 2 $\mu\text{L}/\text{min}$ and 10 x 2 $\mu\text{L}/\text{min}$).

Two-photon excited photoluminescence

The set-up for TPPL has been described previously.^[19] Briefly, the experiments use a scanning stage confocal microscope. They are performed in air and at ambient temperature in a droplet of sample deposited on a clean coverslip. The sample is illuminated by a titanium-sapphire femtosecond laser (wavelength 800 nm, 80 MHz repetition rate, 150fs pulse duration) through a high numerical aperture water-immersion objective (N.A.=1.2, 60x Nikon). The luminescence of the particles diffusing inside the excitation volume is collected by the same objective and is directed to a 50% fiber coupler after passing through a dichroic mirror (Semrock FF720SDiO1). Matching between the collected beam profile and the fiber core is ensured by a telescope. The collected light is filtered by a short pass filter (Semrock FF016-680/SP) to remove the residual laser light.

One fiber of the coupler is directly connected to an avalanche photodiode. This path allows detecting the bursts of luminescence of the freely diffusing particles. A long additional fiber (length 100 m) is inserted in the path of the second fiber before the signal is detected by a second avalanche photodiode. This path is devoted to the spectral analysis of the bursts of luminescence by the photo time-of-flight method as already described previously.^[19,20] In PTOFS, the photons that travel into the long fiber have a transit time that depends on their wavelength according to the chromatic dispersion in the long fiber. As a result, the light flash that is detected by the APD connected to this path is stretched and the profile of the output signal is directly related to the spectrum of the incoming flash. The recording of the temporal traces of the emitted photons uses a time-correlated single photon counting. The correlation function used for FCS and the spectra of the data are derived by post processing with home-made software.

Acknowledgments

This work was supported by Dstl (UK) in the framework of the France-UK Ph.D. programme. AD and MW acknowledge funding by the Agence Nationale de la Recherche (France), grant ANR-2010-JCJC-1005-1 (COMONSENS).

Bibliography

- [1] L. Di Michele, E. Eiser, *Phys. Chem. Chem. Phys.* **2013**, *15*, 3115.
- [2] C. A. Mirkin, R. L. Letsinger, R. C. Mucic, J. J. Storhoff, *Nature* **1996**, *382*, 607–609.
- [3] A. P. Alivisatos, K. P. Johnsson, X. Peng, T. E. Wilson, C. J. Loweth, M. P. Bruchez, P. G. Schultz, *Nature* **1996**, *382*, 609–611.
- [4] A. Heuer-Jungemann, A. H. El-Sagheer, P. M. Lackie, T. Brown, A. G. Kanaras, *Nanoscale* **2016**, *8*, 16857–16861.

- [5] W. Yan, L. Xu, C. Xu, W. Ma, H. Kuang, L. Wang, N. A. Kotov, *J. Am. Chem. Soc.* **2012**, *134*, 15114–15121.
- [6] J. Liu, Y. Geng, E. Pound, S. Gyawali, J. R. Ashton, J. Hickey, A. T. Woolley, J. N. Harb, *ACS Nano* **2011**, *5*, 2240–2247.
- [7] Z. Qian, D. S. Ginger, *J. Am. Chem. Soc.* **2017**, *139*, 5266–5276.
- [8] C. Zhang, R. J. Macfarlane, K. L. Young, C. H. J. Choi, L. Hao, E. Auyeung, G. Liu, X. Zhou, C. A. Mirkin, *Nat. Mater.* **2013**, *12*, 741–746.
- [9] R. J. Macfarlane, M. N. O'Brien, S. H. Petrosko, C. A. Mirkin, *Angew. Chemie Int. Ed.* **2013**, *52*, 5688–5698.
- [10] J. I. L. Chen, Y. Chen, D. S. Ginger, *J. Am. Chem. Soc.* **2010**, *132*, 9600–9601.
- [11] S. E. Lee, Q. Chen, R. Bhat, S. Petkiewicz, J. M. Smith, V. E. Ferry, A. L. Correia, A. P. Alivisatos, M. J. Bissell, *Nano Lett.* **2015**, *15*, 4564–4570.
- [12] N. Seow, Y. N. Tan, L.-Y. L. Yung, X. Su, *Sci. Rep.* **2016**, *5*, 18293.
- [13] J. R. G. Navarro, M. H. V Werts, *Analyst* **2013**, *138*, 583–592.
- [14] R. Fernandes, N. R. Smyth, O. L. Muskens, S. Nitti, A. Heuer-Jungemann, M. R. Ardern-Jones, A. G. Kanaras, *Small* **2015**, *11*, 713–721.
- [15] N. Fairbairn, A. Christofidou, A. G. Kanaras, T. A. Newman, O. L. Muskens, *Phys. Chem. Chem. Phys.* **2013**, *15*, 4163–4168.
- [16] C. Andreou, V. Neuschmelting, D.-F. Tschaharganeh, C.-H. Huang, A. Oseledchyk, P. Iacono, H. Karabeber, R. R. Colen, L. Mannelli, S. W. Lowe, et al., *ACS Nano* **2016**, *10*, 5015–5026.
- [17] O. Akcikir, J. Therrien, G. Belomoin, N. Barry, J. D. Muller, E. Gratton, M. Nayfeh, *Appl. Phys. Lett.* **2000**, *76*, 1857–1859.
- [18] M. Loumagne, A. Richard, J. Laverdant, D. Nutarelli, A. Débarre, *Nano Lett.* **2010**, *10*, 2817–24.
- [19] M. Loumagne, J. R. G. Navarro, S. Parola, M. H. V. Werts, A. Débarre, *Nanoscale* **2015**, *7*, 9013–9024.
- [20] M. Loumagne, P. Vasanthakumar, A. Richard, A. Débarre, *ACS Nano* **2012**, *6*, 10512–10523.
- [21] P. K. Jain, W. Huang, M. A. El-Sayed, *Nano Lett.* **2007**, *7*, 2080–2088.
- [22] B. M. Reinhard, M. Siu, H. Agarwal, A. P. Alivisatos, J. Liphardt, *Nano Lett.* **2005**, *5*, 2246–2252.

- [23] M. Loumagne, C. Midelet, T. Doussineau, P. Dugourd, R. Antoine, M. Stamboul, A. Débarre, M. H. V. Werts, *Nanoscale* **2016**, 8, 6555–6570.
- [24] X. Lan, Z. Chen, B.-J. Liu, B. Ren, J. Henzie, Q. Wang, *Small* **2013**, 9, 2308–2315.
- [25] G. Deželić, J. P. Kratochvil, *Kolloid-Zeitschrift* **1960**, 173, 38–48.
- [26] C. F. Bohren, D. R. Huffman, *Absorption and Scattering of Light by Small Particles*, Wiley Interscience, New York, **1983**.
- [27] M. A. Yurkin, A. G. Hoekstra, *J. Quant. Spectrosc. Radiat. Transf.* **2011**, 112, 2234–2247.
- [28] B. T. Draine, P. J. Flatau, *J. Opt. Soc. Am. A* **1994**, 11, 1491–1499.
- [29] B. Khlebtsov, A. Melnikov, V. Zharov, N. Khlebtsov, *Nanotechnology* **2006**, 17, 1437–1445.
- [30] A. Dhawan, S. J. Norton, M. D. Gerhold, T. Vo-Dinh, *Opt. Express* **2009**, 17, 9688–9703.
- [31] V. Myroshnychenko, J. Rodríguez-Fernández, I. Pastoriza-Santos, A. M. Funston, C. Novo, P. Mulvaney, L. M. Liz-Marzán, F. J. García de Abajo, *Chem. Soc. Rev.* **2008**, 37, 1792.
- [32] R. Esteban, A. G. Borisov, P. Nordlander, J. Aizpurua, *Nat. Commun.* **2012**, 3, 825.
- [33] M. H. V. Werts, V. Raimbault, R. Texier-Picard, R. Poizat, O. Français, L. Griscom, J. R. G. Navarro, *Lab Chip* **2012**, 12, 808–820.
- [34] Z. Guan, L. Polavarapu, Q. H. Xu, *Langmuir* **2010**, 26, 18020–18023.
- [35] H. Wang, T. B. Huff, D. A. Zweifel, W. He, P. S. Low, A. Wei, J.-X. Cheng, *Proc. Natl. Acad. Sci.* **2005**, 102, 15752–15756.
- [36] M. Yorulmaz, S. Khatua, P. Zijlstra, A. Gaiduk, M. Orrit, *Nano Lett.* **2012**, 12, 4385–4391.
- [37] A. Tcherniak, S. Dominguez-Medina, W. S. Chang, P. Swanglap, L. S. Slaughter, C. F. Landes, S. Link, *J. Phys. Chem. C* **2011**, 115, 15938–15949.
- [38] D. Huang, C. P. Byers, L. Y. Wang, A. Hoggard, B. Hoener, S. Dominguez-Medina, S. Chen, W. S. Chang, C. F. Landes, S. Link, *ACS Nano* **2015**, 9, 7072–7079.
- [39] M. Loumagne, G. Laurent, M. H. V. Werts, A. Débarre, *Phys. Chem. Chem. Phys.* **2016**, 18, 33264–33273.
- [40] Z. Guan, N. Gao, X.-F. Jiang, P. Yuan, F. Han, Q.-H. Xu, *J. Am. Chem. Soc.* **2013**, 135, 7272–7277.

- [41] M. B. Mohamed, V. Volkov, S. Link, M. A. El-Sayed, *Chem. Phys. Lett.* **2000**, 317, 517–523.
- [42] K. Imura, T. Nagahara, H. Okamoto, *J. Am. Chem. Soc.* **2004**, 126, 12730–12731.
- [43] H. Hu, H. Duan, J. K. W. Yang, Z. X. Shen, *ACS Nano* **2012**, 6, 10147–10155.
- [44] E. Dulkeith, T. Niedereichholz, T. Klar, J. Feldmann, G. von Plessen, D. Gittins, K. Mayya, F. Caruso, *Phys. Rev. B* **2004**, 70, 205424.
- [45] J. Mertens, M.-E. Kleemann, R. Chikkaraddy, P. Narheng, *Nano Lett.* **2017**, DOI 10.1021/acs.nanolett.7b00332.
- [46] E. L. Elson, D. Magde, *Biopolymers* **1974**, 13, 1–27.
- [47] D. Magde, E. L. Elson, W. W. Webb, *Biopolymers* **1974**, 13, 29–61.
- [48] J. Ries, P. Schwille, *BioEssays* **2012**, 34, 361–368.
- [49] G. Schneider, G. Decher, N. Nerambourg, R. Praho, M. H. V Werts, M. Blanchard-Desce, *Nano Lett.* **2006**, 6, 530–6.
- [50] N. Nerambourg, R. Praho, M. H. V. Werts, D. Thomas, M. Blanchard-Desce, *Int. J. Nanotechnol.* **2008**, 5, 722.
- [51] J. R. G. Navarro, M. Plugge, M. Loumagne, A. Sanchez-Gonzalez, B. Mennucci, A. Débarre, A. M. Brouwer, M. H. V Werts, *Photochem. Photobiol. Sci.* **2010**, 9, 1042–54.
- [52] C. M. Pieper, J. Enderlein, *Chem. Phys. Lett.* **2011**, 516, 1–11.
- [53] M. M. Tirado, C. L. Martínez, J. G. de la Torre, *J. Chem. Phys.* **1984**, 81, 2047–2052.
- [54] M. J. Urban, I. T. Holder, M. Schmid, V. Fernandez Espin, J. Garcia de la Torre, J. S. Hartig, H. Cölfen, *ACS Nano* **2016**, 10, 7418–7427.
- [55] J. Midelet, A. H. El-Sagheer, T. Brown, A. G. Kanaras, M. H. V. Werts, *Part. Part. Syst. Character.* **2017**, 1700095.
- [56] C. M. Alexander, J. Goodisman, *J. Colloid Interface Sci.* **2014**, 418, 103–112.
- [57] C. M. Alexander, J. C. Dabrowiak, J. Goodisman, *J. Colloid Interface Sci.* **2013**, 396, 53–62.
- [58] J. Walter, T. Thajudeen, S. Süß, D. Segets, W. Peukert, *Nanoscale* **2015**, 7, 6574–6587.
- [59] T. Detloff, T. Sobisch, D. Lerche, *Part. Part. Syst. Character.* **2006**, 23, 184–187.
- [60] K. L. Planken, H. Cölfen, *Nanoscale* **2010**, 2, 1849.
- [61] P. K. Harimech, S. R. Gerrard, A. H. El-Sagheer, T. Brown, A. G. Kanaras, *J. Am. Chem. Soc.* **2015**, 137, 9242–9245.

- [62] M. P. Shortell, R. A. Hewins, J. F. S. Fernando, S. L. Walden, E. R. Waclawik, E. A. Jaatinen, *Opt. Express* **2016**, 24, 17090.
- [63] P. H. C. Eilers, *Anal. Chem.* **2003**, 75, 3631–3636.
- [64] R. Schafer, *IEEE Signal Process. Mag.* **2011**, 28, 111–117.
- [65] F. Pérez, B. E. Granger, J. D. Hunter, *Comput. Sci. Eng.* **2011**, 13, 13–21.
- [66] J. P. Brody, P. Yager, *Sensors Actuators A Phys.* **1997**, 58, 13–18.
- [67] J. Turkevich, P. C. Stevenson, J. Hillier, *Discuss. Faraday Soc.* **1951**, 11, 55.
- [68] G. Frens, *Nat. Phys. Sci.* **1973**, 241, 20–22.
- [69] G. Schmid, A. Lehnert, *Angew. Chemie Int. Ed. English* **1989**, 28, 780–781.
- [70] S. J. Barrow, A. M. Funston, X. Wei, P. Mulvaney, *Nano Today* **2013**, 8, 138–167.

Supporting information

Synthesis and characterization of ssDNA-AuNP monoconjugates and DNA-linked AuNP dimers

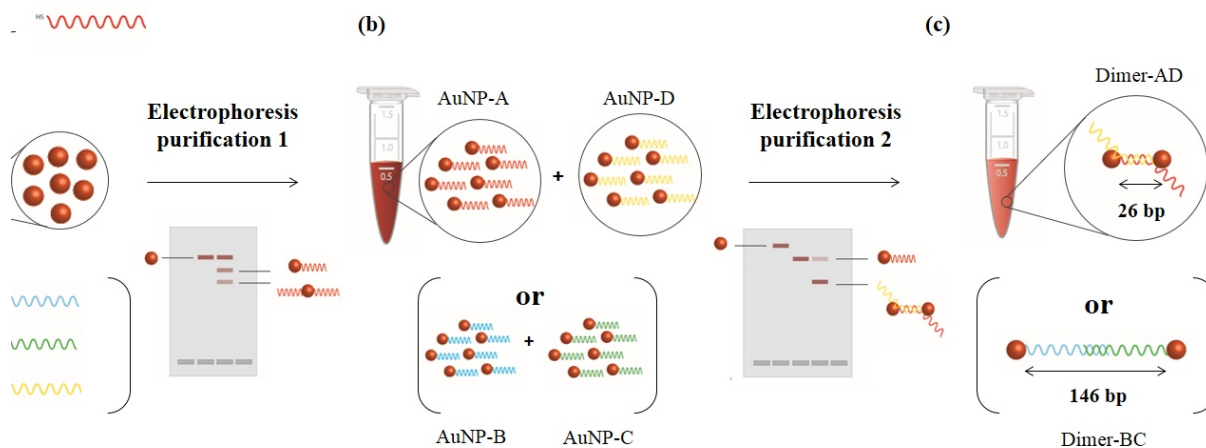


Figure S1. Schematic representation of the synthesis and purification of the four monomer ssDNA-AuNP monoconjugates, and the two DNA-linked AuNP dimers with interparticle links of 26 ('short link' AD) resp. 146 bp ('long link' BC).

Spherical gold nanoparticles of 12 ± 3 nm diameter were synthesised using the well established Turkevich et al.^[67] method modified later on by Frens et al.^[68] A solution of sodium tetrachloroaurate (100 mL, 1 mM) was brought to 100 °C with mild stirring. Once boiling, a warm solution of trisodium citrate (5 mL, 2% wt/V) was added with vigorous stirring. A colour change occurred from yellow to colourless to dark purple and finally to red. Once the red colour was obtained, the boiling and the stirring were maintained for 15 additional minutes before allowing the reaction mixture to cool down to room temperature. Transmission electron microscopy (TEM) analysis of the citrate AuNPs is shown in Figure S2.

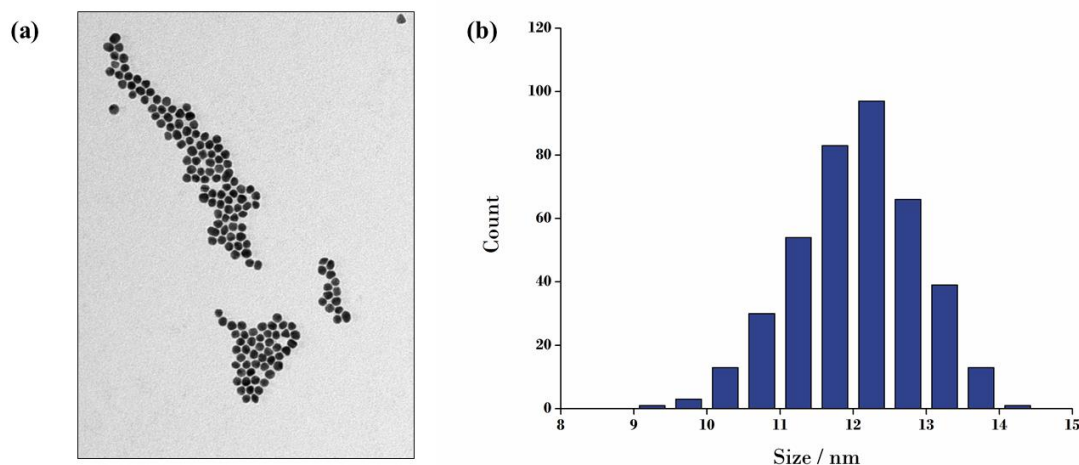


Figure S2. (a) TEM picture and (b) Size distribution histogram of 12 ± 3 nm gold nanoparticles synthesised using the Turkevich method. Scale bar is 200 nm and total count is 400 particles

Particles were then incubated with BSPP to increase the stability by replacing the citrate (15 mg).^[69] After overnight stirring, NaCl was added to aggregate the particles. Aggregation was confirmed by a colour change from red to dark blue. The aggregated particles were then subject to centrifugation at $25,000 \times g$ for 30 min at 25 °C and re-suspended in phosphate buffer (20 mM phosphate, 5 mM NaCl) prior to DNA functionalization.

Two types of dimers with different linker lengths were assembled through DNA hybridisation. AuNPs (12 ± 3 nm) dissolved in phosphate buffer were incubated in a 1:1 ratio with thiol-functionalized oligonucleotides (A, B, C or D, Supporting Info, Figure S3a). All the oligonucleotides initially contained a disulfide terminated group, which was deprotected by adding a BSPP solution (10 μ L, 1 mg/20 μ L). This mixture was left to react while shaking for 1 h prior to being added to the nanoparticle solution. The AuNP-oligonucleotide monoconjugates of each strand were purified using agarose gel electrophoresis (1.75% in 0.5xTBE) run at 100 V for 45 minutes. After diffusion from the gel the monoconjugates were centrifuged for 20 min at $25\,000 \times g$ and redispersed in hybridization buffer (50 μ L, 6 mM phosphate, 80 mM NaCl). Particles bearing the strands A and B were mix as well as the one bearing C and D in a ratio 1:1. Dimer hybridisation was then carried out by heating up the solutions to 75°C and leaving them to cool down to room temperature slowly. After a second agarose gel electrophoresis (1.75% in 0.5 x TBE) run at 100 V for an hour final dimers AD and BC were extracted from the gel. A last centrifugation was performed for 30min at $25\,000 \times g$ and the dimers were redispersed in Mili-Q water.

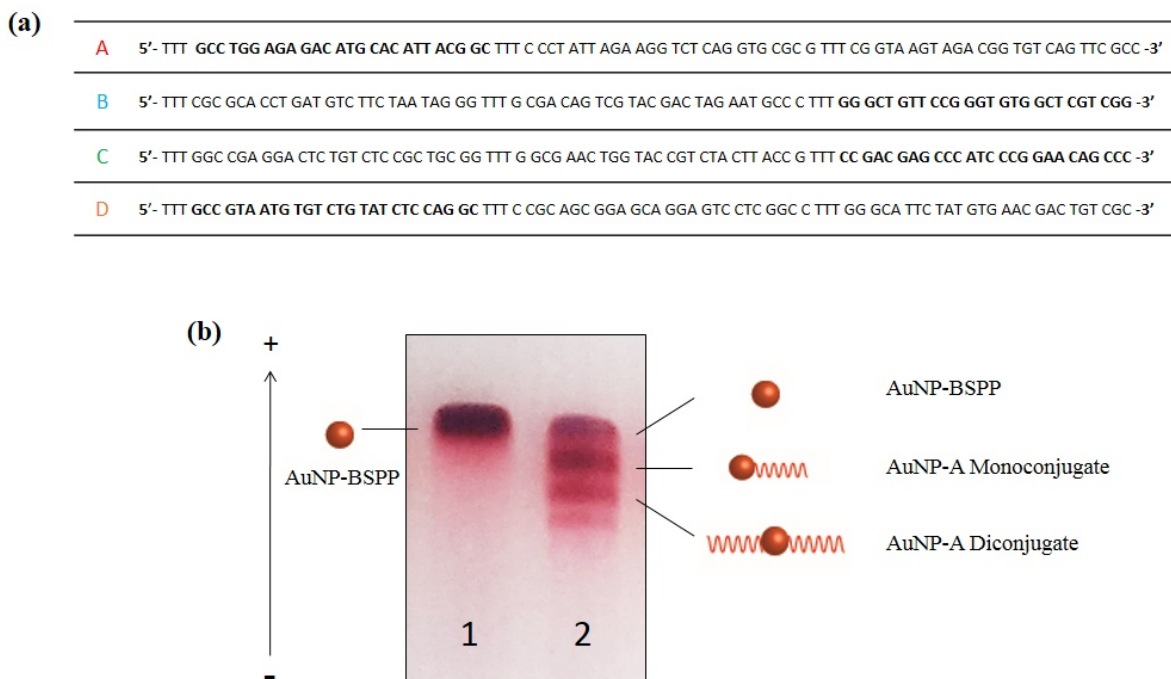


Figure S3. (a) Single stranded DNA sequences used to form DNA-linked gold nanoparticles dimers. All 5' have a protected thiol group. The parts in bold are complementary to each other for A and D and for B and C. (b) Agarose gel electrophoresis (1.75% in 0.5xTBE) for the separation of ssDNA-AuNP monoconjugates. With Lane 1- 12 ± 3 nm AuNP-BSPP and Lane 2 – AuNP-ssDNA conjugates

The ssDNA-AuNP monoconjugates and DNA-linked dimers were analyzed by agarose gel electrophoresis. As seen in the Supporting Info, Figure S4a, both the short-link and long-link AuNP dimers (Lane 3 - AD and Lane 4 - BC, respectively) are delayed compared to BSPP-coated AuNPs or ssDNA-AuNP monoconjugates due to the increase in size of the assemblies. A further delay is noticed for BC dimers compared to AD dimers. This is attributed to their larger interparticle distance. After purification the dimer assemblies were characterised using transmission electron microscopy (Supporting Info, Figure S4b).

All samples were deposited on Carbon Film 400 Mesh Copper grids for transmission electron microscopy (TEM) imaging. All TEM images were obtained on a Hitachi H7000 transmission electron microscope operating at a bias voltage of 75 kV. On the TEM images the difference between the interparticle distance (26 bp for dimer-AD and 146 bp for dimer-BC) cannot be noticed. Since in DNA, a sequence of 10 bp ideally corresponds to a length of 3.4 nm, AuNP dimers should be theoretically separated by 8.84 and 49.6 nm. However, the TEM image shows AuNPs in the dimers in close proximity. This observation is the result of the capillary drying forces and Van der Waals nanoparticle attractions occurring during the TEM grid drying and is not representative to the distance in solution.^[70]

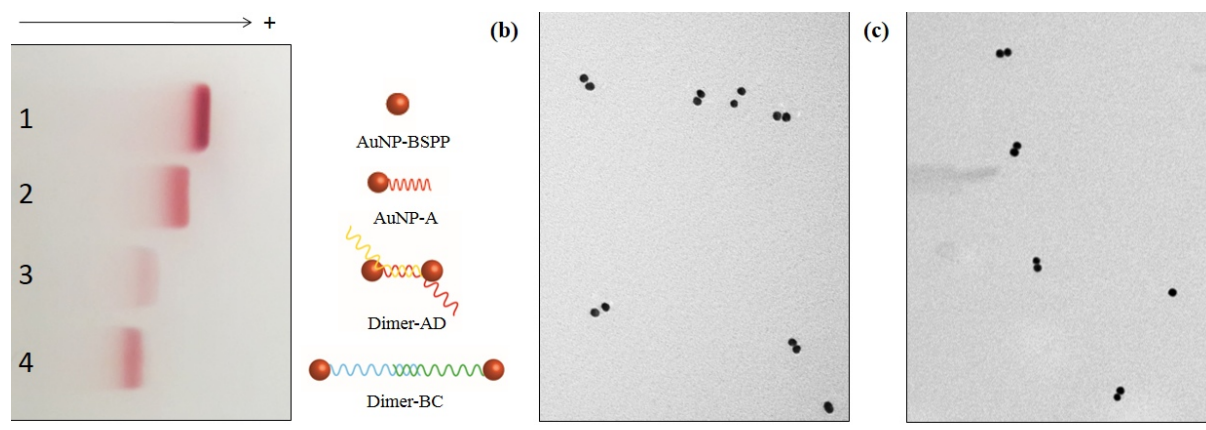


Figure S4. (a) Agarose gel electrophoresis (1.75% in 0.5xTBE) for the purification of DNA-AuNP dimers. With Lane 1- 12 ± 3 nm BSPP AuNPs, Lane 2- Strand A ssDNA-AuNP monoconjugates (AuNP-A), Lane 3- AD DNA-AuNP dimers and Lane 4 - BC DNA-AuNP dimers. TEM images: (b) AD and (c) BC DNA-linked 12 nm AuNP dimers. Scale bars are 200 nm.

Whittaker-Eilers smoother

The Whittaker-Eilers smoother was implemented in Python 3.6.1 with the numpy 1.12.1 and scipy 0.19.0 extensions (Anaconda Python Distribution, Anaconda, Inc., Austin, Texas, USA). The original Matlab program by Eilers^[63] uses the sparse Cholesky solver for solving the matrix equation involved in the smoothing procedure, but since a sparse Cholesky solver is not available in the 'scipy' sparse matrix library, we chose the sparse LU-decomposition based solver instead ('scipy.sparse.linalg.splu'). Our Python implementation was tested with the data provided with the original publication,^[63] and gave identical smoothing results. The core function is given below.

```

import numpy as np
import scipy.sparse as sparse
from scipy.sparse.linalg import splu

def speyediff(N, d, format='csc'):
    """
    Construct a d-th order sparse difference matrix based on
    an initial N x N identity matrix (utility function)

    Final matrix (N-d) x N
    """

    assert not (d < 0), "d must be non negative"
    shape = (N-d, N)
    diagonals = np.zeros(2*d + 1)
    diagonals[d] = 1.
    for i in range(d):
        diff = diagonals[:-1] - diagonals[1:]
        diagonals = diff
    offsets = np.arange(d+1)
    spmat = sparse.diags(diagonals, offsets, shape, format=format)
    return spmat

def whittaker_smooth(y, lmbd, d = 2):
    """
    Implementation of the Whittaker smoothing algorithm,
    based on the work by Eilers [1].

    [1] P. H. C. Eilers, "A perfect smoother", Anal. Chem. 2003, (75), 3631-3636

    The larger 'lmbd', the smoother the data.
    For smoothing of a complete data series, sampled at equal intervals

    This implementation uses sparse matrices enabling high-speed processing
    of large input vectors

    -----

    Arguments :

    y          : vector containing raw data
    lmbd       : parameter for the smoothing algorithm (roughness penalty)
    d          : order of the smoothing

    -----

    Returns :

    z          : vector of the smoothed data.
    """

    m = len(y)
    E = sparse.eye(m, format='csc')
    D = speyediff(m, d, format='csc')
    coefmat = E + lmbd * D.conj().T.dot(D)
    z = splu(coefmat).solve(y)
    return z

```

Quantum-efficiency normalized light scattering spectrum from Mie theory

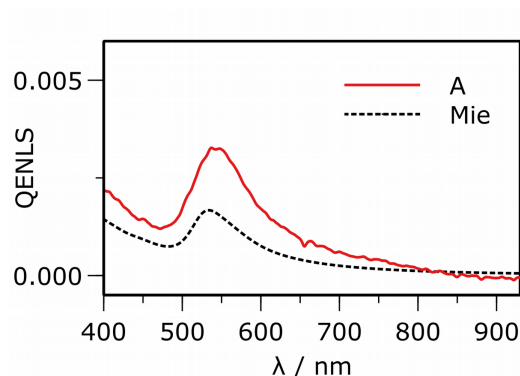


Figure S5. QENLS spectrum calculated using Mie theory and idealized 12 nm gold nanospheres in pure water (dotted line), comparison with experimental QENLS spectrum for monomeric "A" DNA-modified AuNPs (solid red line). The spectra have not been re-scaled, and come directly from theory and experiment, respectively, demonstrating that they are within the same order of magnitude (scattering efficiency at maximum $\sim 10^{-3}$)

Microfluidic diffusion coefficient measurements

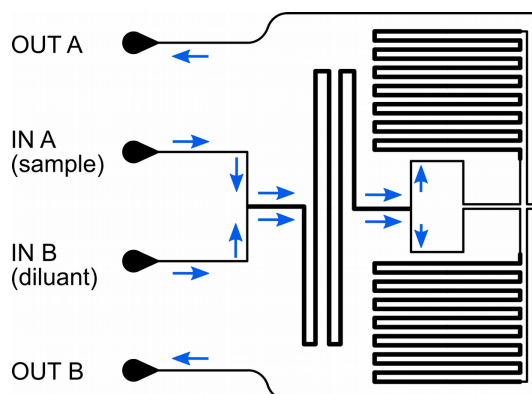


Figure S6. Microfluidic circuit used for the determination of diffusion coefficients. Blue arrows indicate fluid flow direction. The length of the flow interaction zone is 50 mm, with width 200 μm and height 140 μm . After splitting the flow, each channel follows a long serpentine channel for additional hydrodynamic resistance.